Supporting Information

Superior Methanol Electrooxidation Performance of (110)-Faceted Nickel Polyhedral Nanocrystals

Junshan Li,[a,b] Yong Zuo,[a,b] Junfeng Liu,[a,b] Xiang Wang,[a,b] Xiaoting Yu,[a,b] Ruifeng Du,[a,b] Ting Zhang,[c] Maria F. Infante-Carrió,[c] Pengyi Tang,[c] Jordi Arbiol,[c,d] Jordi Llorca,[e] Zhishan Luo,[a*] Andreu Cabot[a,d,*]

a Catalonia Institute for Energy Research - IREC, Sant Adrià de Besòs, Barcelona, 08930, Spain

b Department of Electronics and Biomedical Engineering, Universitat de Barcelona, 08028 Barcelona, Spain

c Catalan Institute of Nanoscience and Nanotechnology (ICN2), CSIC and BIST, Campus UAB, Bellaterra, 08193 Barcelona, Spain

d ICREA, Pg. Lluís Companys 23, 08010 Barcelona, Spain

e Institute of Energy Technologies, Department of Chemical Engineering and Barcelona Research Center in Multiscale Science and Engineering. Universitat Politècnica de Catalunya, EEBE, 08019 Barcelona, Spain

Z. Luo current address: Department of Chemistry, Southern University of Science and Technology (SUSTech), Shenzhen, Guangdong 518055, P. R. China.

Corresponding Author

* Andreu Cabot: acabot@irec.cat

* Zhishan luo: luozs@mail.sustc.edu.cn

Contents

1. EELS compositional maps

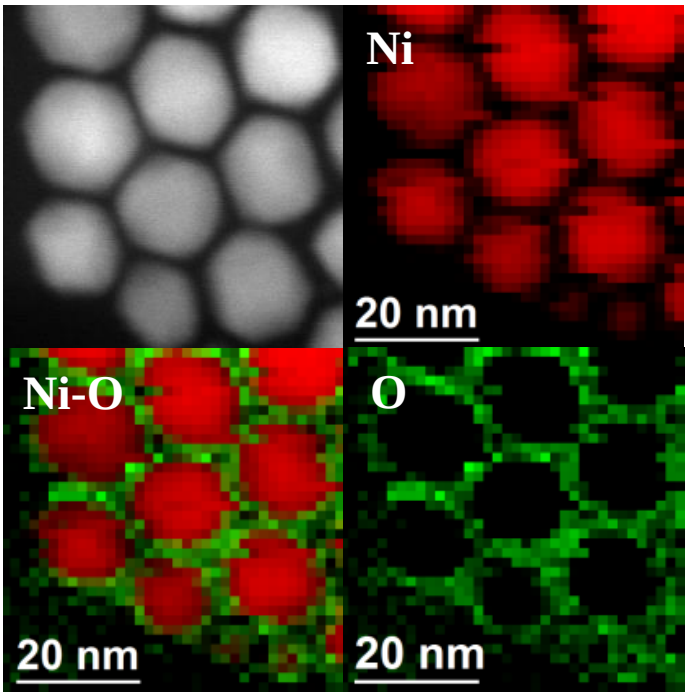

Figure S1. EELS compositional maps for Ni (red) and O (green) obtained from Ni polyhedral NCs.

2. XPS

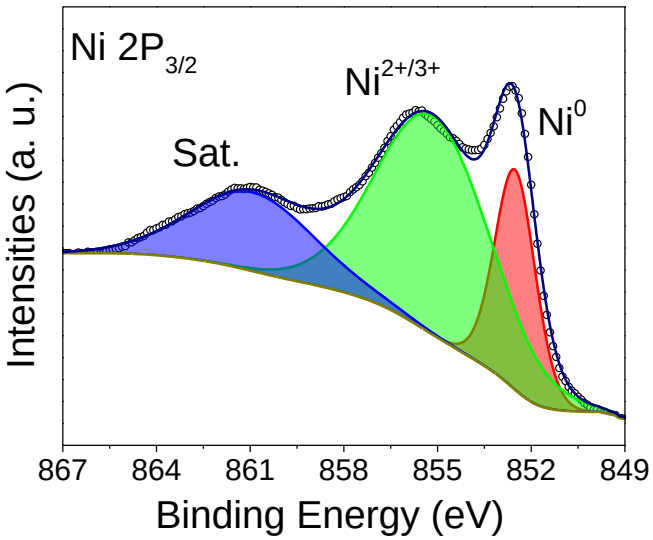

Figure S2. Ni 2p3/2 region of the XPS spectrum of Ni polyhedral NCs.

3. FTIR Spectra

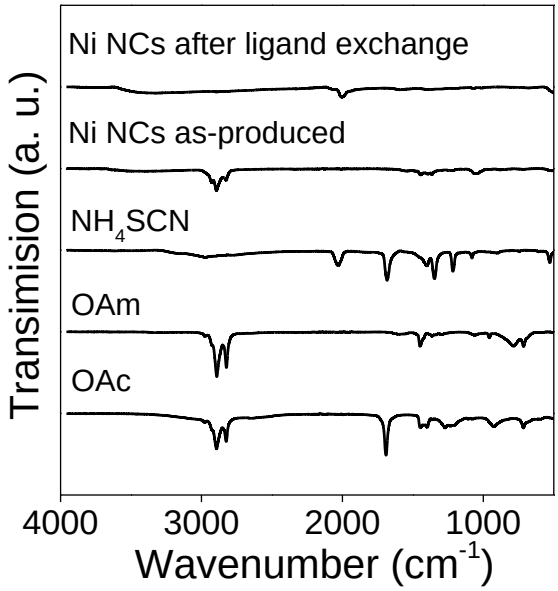

Figure S3. FTIR spectra of the Ni polyhedral NCs before and after ligand exchange. Experimental reference spectra for OAc, OAm and NH_4SCN are also included.

4. Ni spherical NCs

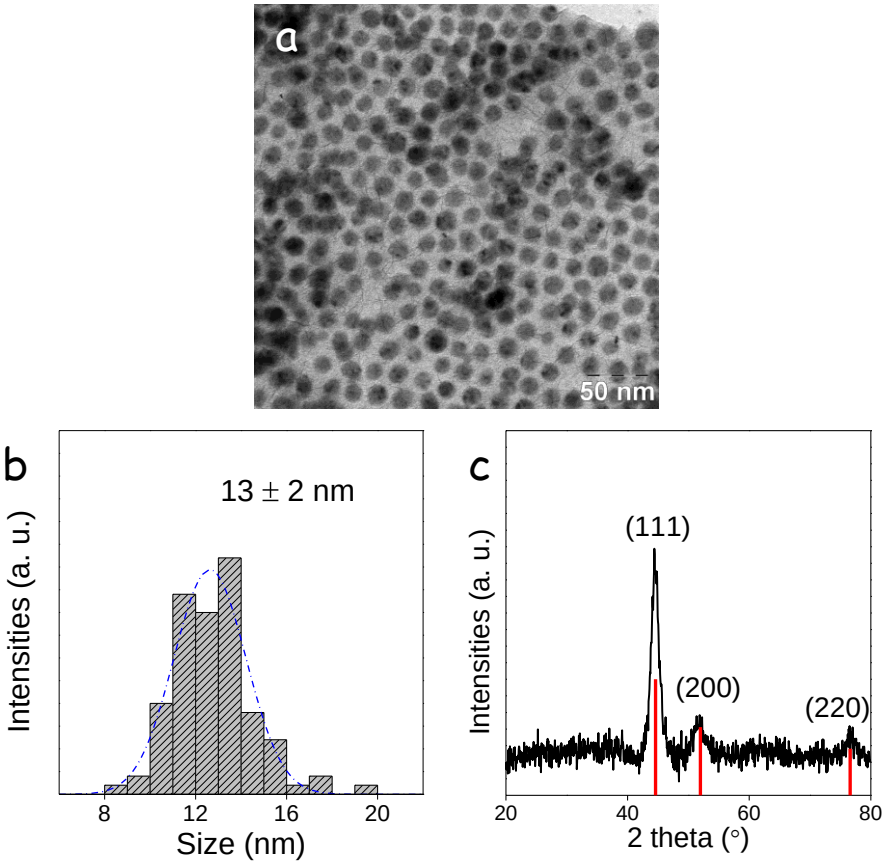

Figure S4. (a) Representative TEM micrograph of Ni spherical NCs. (b) Their size distribution histogram. (c) XRD pattern of Ni spherical NCs including the JCPDS 01-070-0989 reference corresponding to the Ni *fcc*-phase.

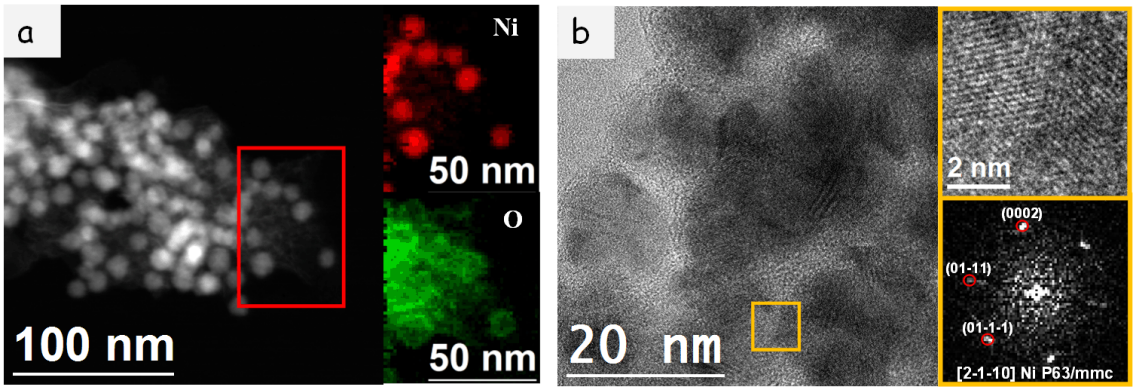

Figure S5. a) ADF-STEM image of several Ni spherical NCs and EELS compositional maps for Ni (red) and O (green). b) HRTEM image of Ni spherical NCs and power spectrum fitting with the Ni *fcc*-phase.

5. Additional electrochemistry data

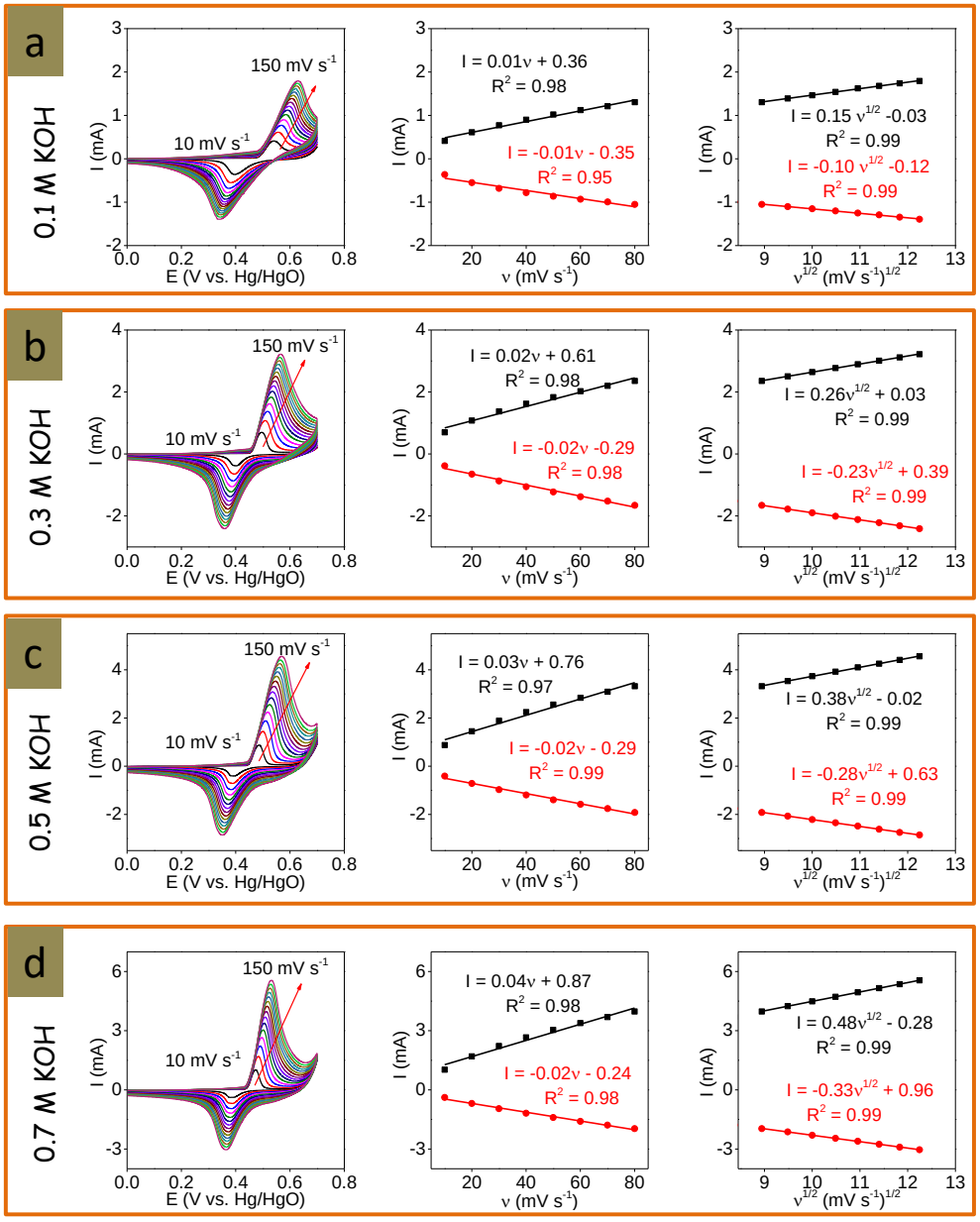

Figure S6. Cyclic voltammograms at increasingly higher potential sweep rates: 10, 20, 30, 40, 50, 60, 70, 80, 90, 100, 110, 120, 130, 140, 150 mV s^{-1} (left column). Linear fitting of anodic and cathodic peak current densities to the scan rates in the low scan rate range (10-80 mV s^{-1}, middle column). Linear fitting of anodic and cathodic peak current densities to the square roots of the scan rates in the high scan rate range (80-150 mV s^{-1}, right column). Data was obtained from an electrode based on Ni polyhedral NCs in a solution containing (a) 0.1 M KOH, (b) 0.3 M KOH (c) 0.5 M KOH (d) 0.7 M KOH.

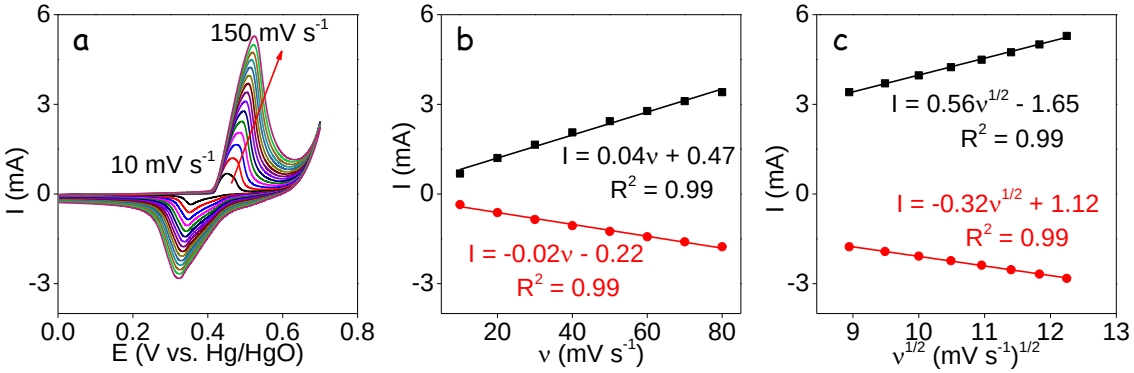

Figure S7. Electrochemical performance of Ni spherical NCs in 1.0 M KOH: (a) Cyclic voltammograms at increasingly higher potentials sweep rates: 10, 20, 30, 40, 50, 60, 70, 80, 90, 100, 110, 120, 130, 140, 150 mV s^{-1}. (b) The linear fitting of anodic and cathodic peak current densities to the scan rates in the low scan rate regime (10-80 mV s^{-1}). (c) The linear fitting of anodic and cathodic peak current densities to the square roots of the scan rates in the high scan rate regime (80-150 mV s^{-1}).

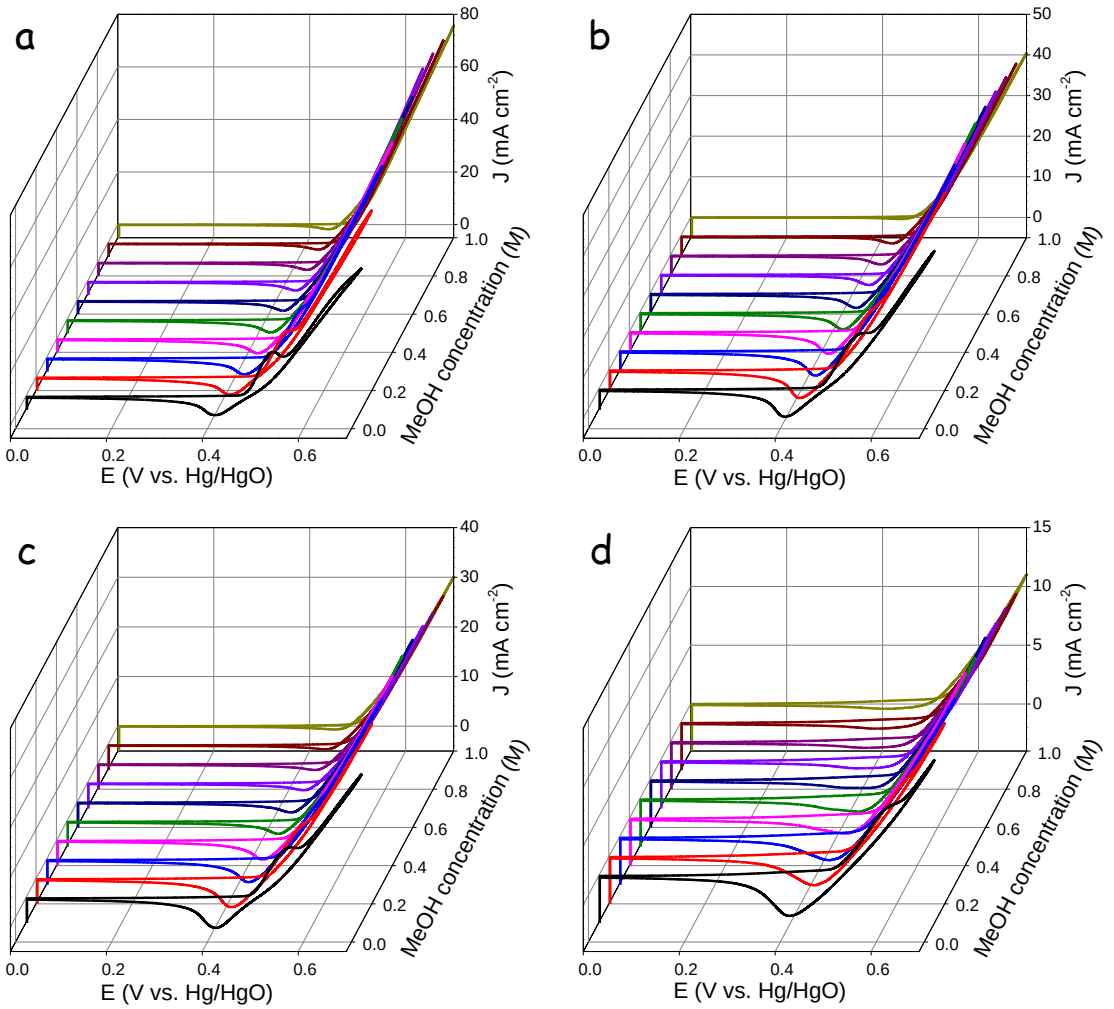

Figure S8. CVs of an electrode based on Ni polyhedral NCs at different methanol concentrations from 0.1 M to 1.0 M at a scan rate of 50 mV s^{-1} in a solution containing (a) 0.1 M KOH, (b) 0.3 M KOH (c) 0.5 M KOH (d) 0.7 M KOH.

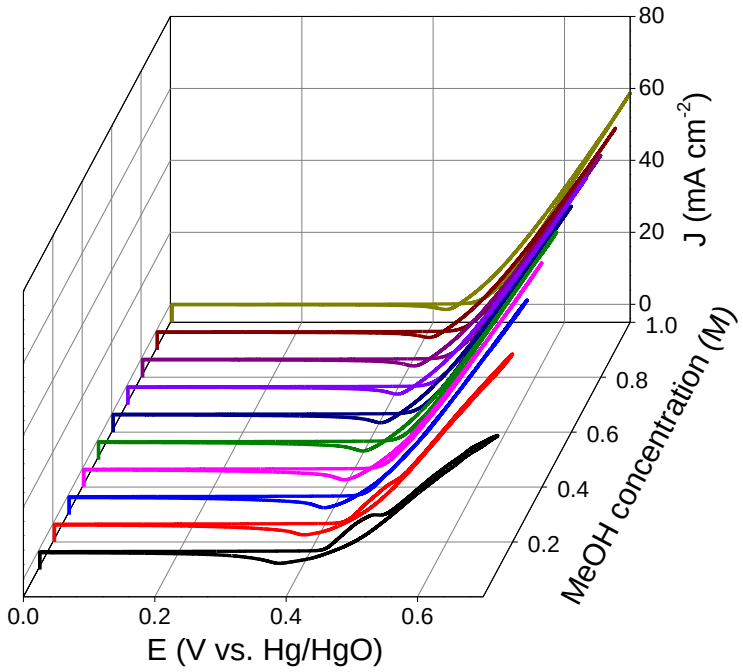

Figure S9. CVs of an electrode based on Ni spherical NCs with different methanol concentrations from 0.1 M to 1.0 M at a scan rate of 50 mV s^{-1} in 1.0 M KOH.

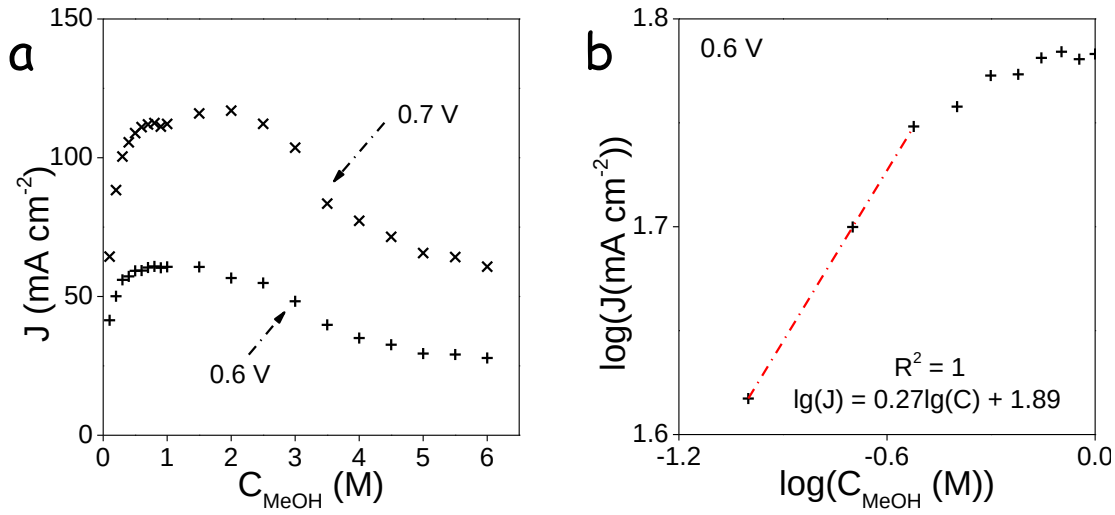

Figure S10. (a) Comparison of the current density at 0.6 V and 0.7 V *vs.* Hg/HgO of Ni polyhedral NCs based electrodes as a function of methanol concentrations from 0.1 M to 6.0 M. (b) logarithmic dependence of the current density (0.6 V vs. Hg/HgO) with the methanol concentration.

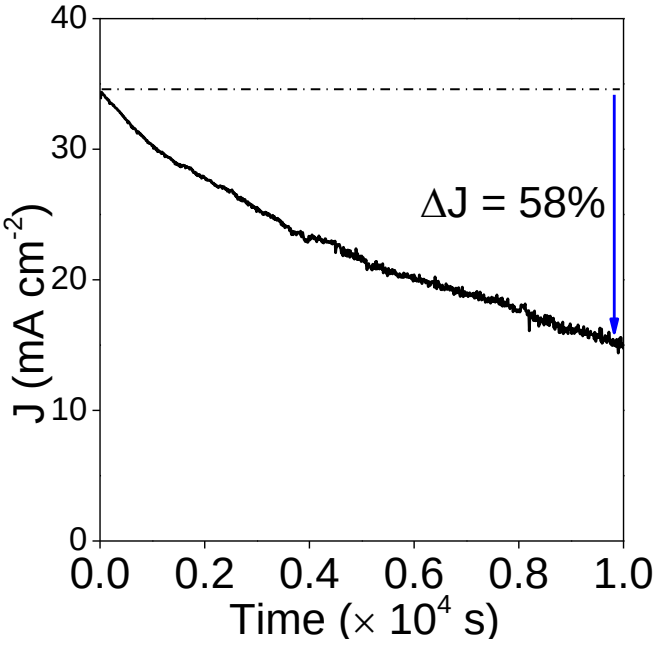

Figure S11. CA response of an electrode based on spherical Ni NCs in 1.0 M KOH and 1.0 M methanol at 0.6 V for 10000 s.

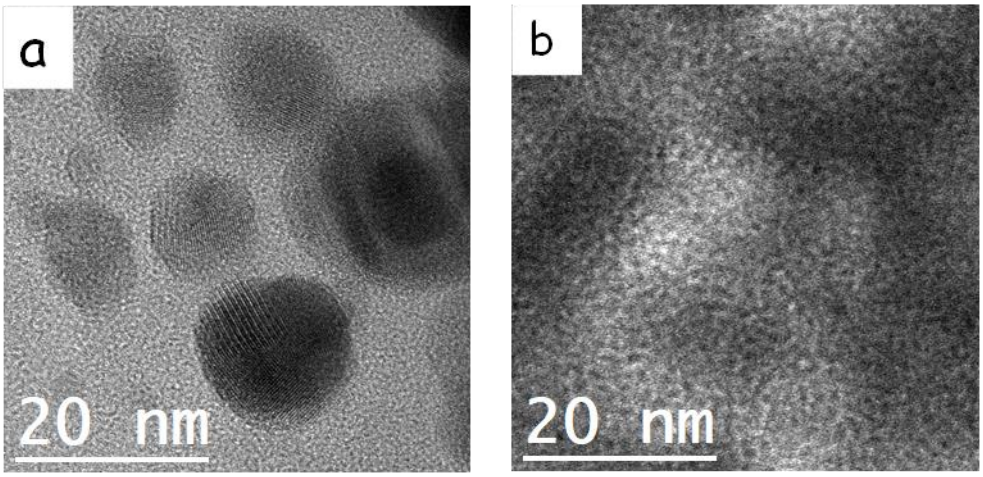

Figure S12. HRTEM micrographs of polyhedral Ni NCs after CA test at 0.6 V vs. Hg/HgO with (a) 10000s and (b) 30000s.

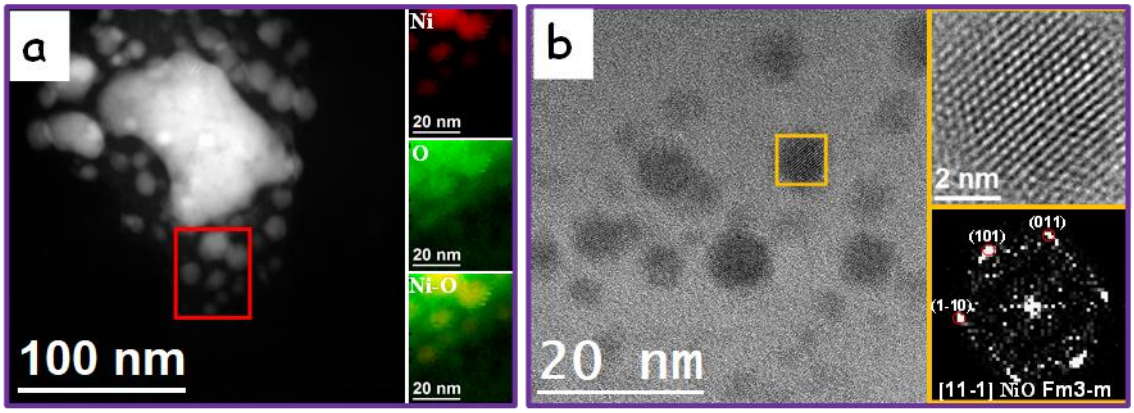

Figure S13. HAADF, EELS-TEM and HRTEM micrographs of polyhedral Ni NCs after 10,000 s CA test at 0.6 V vs. Hg/HgO. (a) EELS chemical composition maps obtained from the red squared area of the STEM micrograph. Individual Ni $L_{2,3}$-edges at 855 eV (red) and O K-edge at 532 eV (green) as well as composites of Ni-O. (b) HRTEM micrograph, detail of the orange squared region and its corresponding power spectrum.

6. Comparison of activity

Table S1. Electrocatalytic performance comparison between electrodes based on Ni polyhedral NCs and other Ni-based electrocatalysts previously reported.

Catalysts	Condition	AP*	Activity		Reference
		V *vs.* RHE	mA cm^{-2}	A mg^{-1}	
CNT-Ni/SiC-700	1.0 M KOH + 1.0 M MeOH	1.84	200	1.00	[1]
Ni nanoparticles@CB	0.4 M KOH + 1.0 M MeOH	1.64	12		[2]
NiFe	0.1 M NaOH + 1.0 M MeOH	1.56	50	1.71	[3]
CNFs-Ni	0.5 M KOH + 1.0 M MeOH	1.47	1.6	0.40	[4]
Ni_2Co_2	1.0 M NaOH + 0.5 M MeOH	1.74	35		[5]
Ni nanoparticles/rGO	1.0 M KOH + 1.0 M MeOH	1.64		1.60	[6]
Ni-Co-P-O	0.5 M KOH + 1.0 M MeOH	1.55	39.9	1.57	[7]
Ni@Ti flakes	1.0 M NaOH + 0.5 M MeOH	1.74	39		[8]
$NiCo_2O_4$/Ni Foam	1.0 M KOH + 0.5 M MeOH	1.55		0.04	[9]
Ni-Ti	0.1 M NaOH + 0.2 M MeOH	1.62	0.5 mA		[10]
Ni-P-O	0.5 M KOH + 1.0 M MeOH	1.57	37.9	1.49	[11]
$Ni_{0.5}Co_{0.5}$	1.0 M NaOH + 0.5 M MeOH	1.69	35		[12]
$Ni_{0.75}Cu_{0.25}$	1.0 M NaOH + 0.5 M MeOH	1.69	45		[13]
NiMn film	1.0 M NaOH + 0.5 M MeOH	1.64	80		[14]
$Ni_{1.7}Sn$@CB	0.5 M KOH + 1.0 M MeOH	1.65	50.9	0.82	[15]
Ni@CNTs	1.0 M KOH + 1.0 M MeOH	1.62	1.5	0.97	[16]
Ni-P nanowires/rGO	1.0 M KOH + 0.5 M MeOH	1.65	16.4	0.12	[17]
Ni spherical NCs @CB	0.5 M KOH + 0.5 M MeOH	1.65	51.2	0.83	[15]
Ni polyhedral NCs @CB	1.0 M KOH + 1.0 M MeOH	1.67	59.4	2.02	This work
Ni polyhedral NCs @CB	1.0 M KOH + 1.0 M MeOH	1.77	95.2	3.12	This work
Ni spherical NCs @CB	1.0 M KOH+ 1.0 M MeOH	1.67	31.3	1.04	This work

*For comparison, the applied potential (AP) was related to RHE using the following equation:

$$E_{RHE} = E^0_{Ref} + E_{Ref} + 0.059 \times pH$$

where E^0_{Ref} is potential of the reference ($E^0_{Ag/AgCl}$ = 0.21 V, $E^0_{Hg/HgO}$ = 0.14 V), E_{Ref} is the potential measured vs. reference, pH is simply calculated from the electrolyte composition (pH = 14 + log[OH^-]).

7. EIS analyses

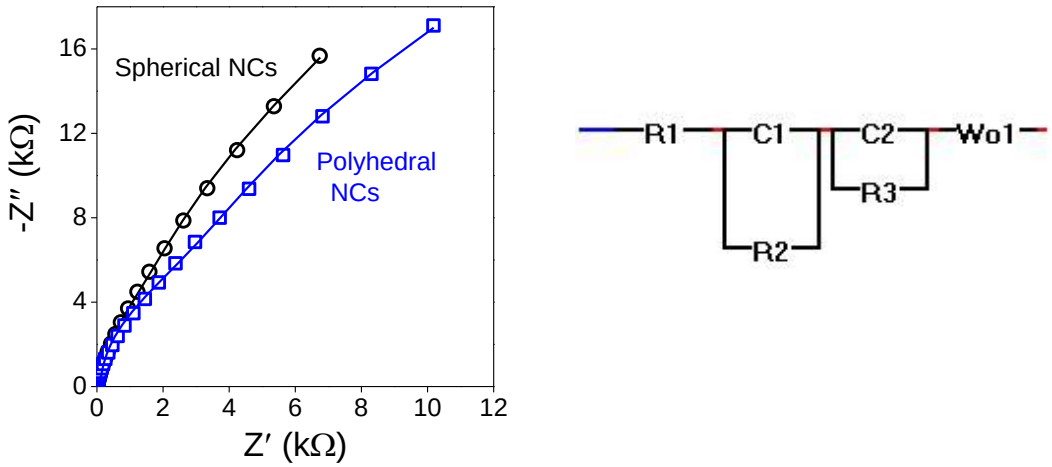

Figure S14. Nyquist plot of the EIS data obtained from electrodes based on polyhedral and spherical Ni NCs. Data was obtained in 1.0 M KOH and 1.0 methanol at open circuit voltage. Graph includes the fitted curves obtained from the model circuit shown on the right. The fitted parameters are displayed in table S2.

Table S2. Parameters obtained from fitting the experimental EIS data with the circuit displayed in figure S12.

Circuit parameter	Polyhedral Ni NCs	Spherical Ni NCs
C1 (F)	8×10^{-5}	1.7×10^{-4}
C2 (F)	1.1×10^{-4}	1.5×10^{-4}
R1 (Ω)	1.3×10^{-12}	1.3×10^{-12}
R2 (Ω)	3200	1580
R3 (Ω)	16610	13130
Wor1	968	795
Woc1	0.26	0.20

8. Reference

1 S. Xie, X.-L. Tong, G.-Q. Jin, Y. Qin and X.-Y. Guo, *J. Mater. Chem. A*, 2013, **1**, 2104–2109.

2 R. M. Abdel Hameed and R. M. El-Sherif, *Appl. Catal. B Environ.*, 2015, **162**, 217–226.

3 S. L. Candelaria, N. M. Bedford, T. J. Woehl, N. S. Rentz, A. R. Showalter, S. Pylypenko, B. A. Bunker, S. Lee, B. Reinhart, Y. Ren, S. P. Ertem, E. B. Coughlin, N. A. Sather, J. L. Horan, A. M. Herring and L. F. Greenlee, *ACS Catal.*, 2017, **7**, 365–379.

4 J. Wang, Q. Zhao, H. Hou, Y. Wu, W. Yu, X. Ji and L. Shao, *RSC Adv.*, 2017, **7**, 14152–14158.

5 X. Cui, W. Guo, M. Zhou, Y. Yang, Y. Li, P. Xiao, Y. Zhang and X. Zhang, *ACS Appl. Mater. Interfaces*, 2015, **7**, 493–503.

6 H. Sun, Y. Ye, J. Liu, Z. Tian, Y. Cai, P. Li and C. Liang, *Chem. Commun.*, 2018, **54**, 1563–1566.

7 Y. Y. Tong, C. D. Gu, J. L. Zhang, H. Tang, Y. Li, X. L. Wang and J. P. Tu, *Electrochim. Acta*, 2016, **187**, 11–19.

8 Q. Yi, W. Huang, J. Zhang, X. Liu and L. Li, *Catal. Commun.*, 2008, **9**, 2053–2058.

9 L. Gu, L. Qian, Y. Lei, Y. Wang, J. Li, H. Yuan and D. Xiao, *J. Power Sources*, 2014, **261**, 317–323.

10 Y. Yu, Q. Yang, X. Li, M. Guo and J. Hu, *Green Chem.*, 2016, **18**, 2827–2833.

11 Y. Y. Tong, C. D. Gu, J. L. Zhang, M. L. Huang, H. Tang, X. L. Wang and J. P. Tu, *J. Mater. Chem. A*, 2015, **3**, 4669–4678.

12 X. Cui, Y. Yang, Y. Li, F. Liu, H. Peng, Y. Zhang and P. Xiao, *J. Electrochem. Soc.*, 2015, **162**, F1415–F1424.

13 X. Cui, P. Xiao, J. Wang, M. Zhou, W. Guo, Y. Yang, Y. He, Z. Wang, Y. Yang, Y. Zhang and Z. Lin, *Angew. Chemie - Int. Ed.*, 2017, **56**, 4488–4493.

14 I. Danaee, M. Jafarian, A. Mirzapoor, F. Gobal and M. G. Mahjani, *Electrochim. Acta*, 2010, **55**, 2093–2100.

15 J. Li, Z. Luo, Y. Zuo, J. Liu, T. Zhang, P. Tang, J. Arbiol, J. Llorca and A. Cabot, *Appl. Catal. B Environ.*, 2018, **234**, 10–18.

16 M. Asgari, M. G. Maragheh, R. Davarkhah and E. Lohrasbi, *J. Electrochem. Soc.*, 2011, **158**, K225.

17 H. Zhang, C. D. Gu, M. L. Huang, X. L. Wang and J. P. Tu, *Electrochem. commun.*, 2013, **35**, 108–111.